Research Square

Preprints are preliminary reports that have not undergone peer review.
They should not be considered conclusive, used to inform clinical practice,
or referenced by the media as validated information.

Application of the Invariance Principle in the Control System of a Fast Pulsator

Mekhti Akhundov

Mehti2001@mail.ru

Kazan Federal University

Elizaveta M. Ganina

Moscow Institute of Physics and Technology

Oleg V. Zhdaneev

Kazan Federal University

Research Article

Keywords: Directional drilling, MWD, Measuring while drilling, High-speed pulser, pulser, direct drive motor

Posted Date: May 25th, 2026

DOI: https://doi.org/10.21203/rs.3.rs-8903852/v1

License: This work is licensed under a Creative Commons Attribution 4.0 International License.
Read Full License

Additional Declarations: No competing interests reported.

Application of the Invariance Principle in the Control System of a Fast Pulsator

M. G. Akhundov[1], E. M. Ganina[2], O. V. Zhdaneev[3]

1. Department of Petroleum Engineering, Kazan Federal University, Kremleskaya str. 18, Kazan, 420008, Russian Federation;
2. Moscow Institute of Physics and Technology, Institutsky lane 9, Dolgoprudny, Moscow region, Russian Federation, 141700;
3. Department of Petroleum Engineering, Kazan Federal University, Kremleskaya str. 18, Kazan, 420008, Russian Federation.

Email address:
Mehti2001@mail.ru (Mekhti Akhundov), ryabko_el@mail.ru (Elizaveta Ganina), Oleg_1978@mail.ru (Oleg Zhdaneev)
ORCID:
0009-0002-9873-7993 (Mekhti Akhundov), 0000-0002-5287-4397 (Oleg Zhdaneev), 0009-0008-3424-8879 (Elizaveta Ganina)

Corresponding author: Mekhti Akhundov

I declare that the authors have no competing interest as defined by Springer, or other interests that might be perceived to influence the results and/or discussion reported in this paper.

To cite this article:
Mekhti Akhundov. (2026). Application of the Invariance Principle in the Control System of a Fast Pulsator.

Abstract: Modern oil and gas drilling, measurement-while-drilling (MWD), and logging-while-drilling (LWD) operations require high-speed transmission of downhole data to the surface to provide geological, petrophysical, drilling, geophysical, and other critical downhole information in real time. The highest mud-pulse telemetry rates currently achieved in the industry are provided by siren-type pulsers developed by major service companies, including Schlumberger, Baker Hughes, Halliburton, and Weatherford. These systems generate phase-modulated pressure signals with sufficient stability for operation in harsh downhole environments. A common architectural characteristic of modern high-speed siren-type pulsers is the use of mechanical speed-reduction stages between the drive motor and the modulating rotor. This approach enables accurate angular positioning of the siren under dynamically varying mud flow rates and rheology, as well as under shocks, vibrations, and stick–slip conditions encountered during drilling. However, such designs inherently increase system complexity using gearboxes, reducers, or equivalent mechanical transmission assemblies. From an engineering standpoint, mechanical speed-reduction mechanisms introduce several well-known drawbacks, including increased part count, additional rotating interfaces, stringent assembly tolerance requirements, and sensitivity to wear caused by abrasive drilling fluids, chemical exposure, and other downhole hazards. In high-speed pulsers, these effects are further amplified by continuous cyclic loading at the modulation frequency, which directly limits working life and overall system reliability. To address these limitations, the proposed solution employs a permanent-magnet synchronous motor operating without a reduction gearbox and is combined with a multiloop covariant vector-control architecture designed to ensure accurate rotor-angle tracking under realistic downhole load-torque disturbances. The central contribution of this work is the first application of the invariance principle to the control of a synchronous motor used in mud-pulse telemetry, enabling phase-stable operation for phase-modulated signaling schemes such as BPSK, QPSK, and MSK. The control system integrates conventional feedback loops with virtual-model functionality and a load-torque invariance block that compensates deterministic, angle-dependent disturbances introduced by the pulser parking mechanism. Experimental results obtained from laboratory and field testing demonstrate significantly reduced phase-tracking errors compared with standard control structures, thereby enabling physical data-transmission rates exceeding 6 bit/s. When combined with data-compression algorithms, the effective telemetry throughput exceeds 50 bit/s, which is sufficient for real-time operation of complex triple-combo LWD toolstrings in horizontal wells. In addition to performance improvements, the pulser features a simplified mechanical design achieved by eliminating the gearbox, resulting in a 15–20% reduction in manufacturing cost and a measurable increase in service life due to fewer wear-prone components. The proposed pulser design can replace existing generation pulsers through adaptation of its mechanical and electrical interfaces to current MWD systems.
Keywords: Directional drilling, MWD, Measuring while drilling, High-speed pulser, pulser, direct drive motor.

Abbreviations:

- BHA - bottom-hole assembly
- EM - electromagnetic
- LWD - logging while drilling
- MWD - measurement while drilling
- BPSK - binary phase-shift keying

- QPSK - quadrature phase-shift keying
- MSK - minimum shift keying
- ROP - rate of penetration
- PMSM - permanent-magnet synchronous motor
- MTBF - mean time between failures
- NPT - non-productive time

Introduction

Horizontal and directional drilling have become the dominant technologies for developing both conventional and unconventional reservoirs [1]. The continued growth of long horizontal laterals, extended-reach trajectories, and multilateral well architectures places stringent requirements on real-time subsurface information and low-latency decision making for geosteering and drilling optimization. In the United States, for example, horizontal and directional wells increased from a minority of completions in 2010 to the majority by the early 2020s, while average drilled footage per well increased substantially (Fig. 1). [2] Extended-reach and multi-lateral drilling trends, as well as the growth of long horizontals, are widely documented in the literature [2-4].

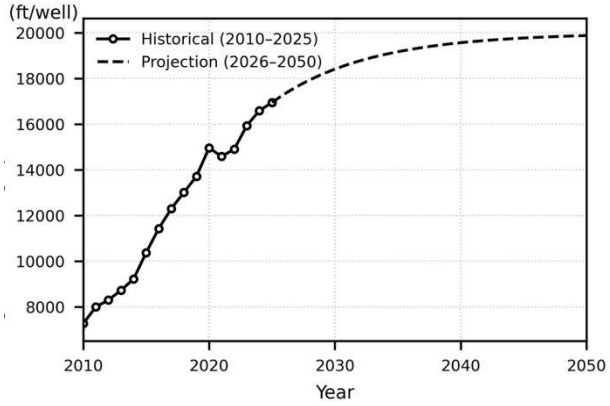


Fig. 1. Average drilled footage per U.S. crude oil and natural gas well (2010–2050): historical data (solid line) and illustrative nonlinear extension to 2050 (dashed line).

Annual values for 2010–2025 are computed from EIA Monthly Energy Review wells-and-footage data as the ratio of total drilled footage to total wells drilled. The 2026–2050 segment is an illustrative non-linear extrapolation; it is calibrated at the 2025 value and conservatively assumes an asymptotic limit of 20,000 ft/well.

Modern bottom-hole assemblies (BHAs) for horizontal sections typically combine measurement-while-drilling (MWD) directional sensors with logging-while-drilling (LWD) tools positioned as close as possible to the bit. These tools provide natural gamma-ray measurements, multi-depth resistivity, density and neutron porosity, and increasingly azimuthal images that support formation-dip estimation and detailed geosteering decisions, [5-8]. The telemetry system also collects drilling diagnostics and tool-health data (temperature, shocks, vibration, and operational status) and organizes them into cyclically transmitted data frames.

The downhole data frame is transmitted to the surface through one of several physical channels, including mud-pulse, electromagnetic (EM), acoustic, and wired drill pipe. Mud-pulse telemetry remains the predominant method for deep and long wells because it is robust over long wellbores, whereas EM and acoustic channels suffer strong attenuation and wired pipe is often non-competitive in cost for many applications. [9] At the same time, the limited bandwidth of mud-pulse telemetry is a major bottleneck for modern MLWD toolstrings that require dense measurements and low latency. [10-13]

The required downhole-to-surface data rate depends on the rate at which sensors move through the formation (rate of penetration, ROP) and on the required sampling density. For a parameter sampled at n samples per meter and encoded using S bytes per sample, the minimum bit rate needed to transmit this parameter in real time can be expressed as: [12-13]

$$V_{bit/sec} = \frac{ROP_{m/h}}{3600} \times n \times S \times 8$$

where:

ROP is the planned rate of penetration, m/h.

n is the required sampling density, samples/m (e. g., 2 samples/ft ≈ 6.56 samples/m).

S is the size of one sample (data point), bytes.

8 is the conversion factor from bytes to bits.

3600 is the conversion factor from hours to seconds (s/h).

Mud-pulse telemetry data rates in practice typically range from 0.5 to 12 bit/s, depending on the pulser type, well depth, mud properties, and the applied encoding/decoding algorithms [14-21]. Rates above approximately 6 bit/s are generally achieved with continuous-wave siren pulsers combined with phase-modulated signaling schemes (BPSK/QPSK/MSK) and advanced surface decoding.

In phase-modulated schemes, rotor-angle tracking error translates directly into carrier phase error, symbol-timing jitter, and increased bit-error rate. High-speed pulsers are therefore limited not only by hydraulics, but also by the ability of the actuator and its control system to maintain phase accuracy under rapidly varying and periodically disturbed load torque. [22-26]

Many existing high-speed pulser designs increase torque and phase stiffness by using mechanical speed-reduction stages (gearboxes, epicyclic reducers, or similar transmissions) between the prime mover (electric motor or hydraulic turbine) and the modulating rotor. Although effective, these mechanisms increase part count and introduce wear-prone interfaces that can reduce reliability under abrasive and high-temperature downhole conditions. An alternative is to remove the gearbox and compensate deterministic disturbances in software using a control structure explicitly designed for position-dependent load torque.

Existing High-Speed Pulsers and Their Limitations

High-speed mud-pulse telemetry solutions are commercially available primarily from major service companies, including Schlumberger, Halliburton, Baker Hughes, and Weatherford. In these systems, high data rates are typically achieved by continuous-wave siren (or rotary-shear) pulsers combined with phase/frequency modulation and advanced surface decoding strategies [27-36].

Table 1 summarizes representative patented architectures of high-speed pulsers from these vendors. A common feature across the reviewed solutions is the use of a mechanical transmission stage (gearbox or reduction drive) between the prime mover (hydraulic turbine or electric motor) and the modulating rotor. This approach increases pulser torque, but it introduces additional dynamics and reliability risks.

Table 1. Patented high-speed mud-pulse pulsers employing mechanical transmission (multi-vendor comparison).

Company	Telemetry system	Modulator type	Reported data rate*	Actuation architecture
Schlumberger	PowerPulse™	Rotary siren (continuous-wave)	3–16 bit/s	Turbine-driven modulator + gear train to alternator (gear train explicitly stated patents US5517464A; US5519668A), [27]
Schlumberger	TeleScope™	High-speed rotary siren (PSK/FSK)	3–16 bit/s	Gear train with 8:1 reduction is explicitly described (US5375098A) [28], [29]
Baker Hughes	aXcelerate™ PLUS	Oscillating shear / siren-like	up to ~20 bit/s	Motor-driven gear system / planetary gear / cam system explicitly disclosed for driving the modulator/rotor (US7280432B2; USRE40944E1) [30], [31]
Weatherford	PulseStar™	Rotary siren pulser	~10–12 bit/s	Motor → reduction drive → siren
Halliburton	HyperPulse™	Fluid-driven mud siren	~12–18 bit/s	Epicyclical/planetary gear reducer explicitly disclosed between turbine rotor and siren rotor; gear ratio governs siren speed (US5583827A; US5586084A) [32-35]
China Oilfield Services Ltd. (COSL)	High-speed shear-valve pulser telemetry	Rotary shear valve (continuous-wave capable)	12 bit/s	Rotary shear valve system

This work	—	Direct-drive rotary siren	>6 bit/s (physical), >50 bit/s (effective)	Direct-drive PMSM (no gearbox)

* Data rates reported in the literature and patents; actual field performance depends on hydraulic and channel conditions.

The main limitations of gearbox-based high-speed pulser architectures that are relevant to phase-modulated telemetry are: additional mechanical complexity and wear-prone components (gears, bearings, and couplings), which can reduce reliability in abrasive drilling environments; backlash and compliance in the transmission, which can degrade phase stiffness and introduce phase jitter at the carrier frequency; higher manufacturing and maintenance cost due to tight tolerances, lubrication requirements, and more complex assembly; position-dependent load-torque disturbances inherent to siren-type modulation and auxiliary mechanisms (e. g., parking mechanisms), which are difficult to fully reject using only high-gain feedback; sensor quantization and speed-estimation noise, which limit the achievable control-loop bandwidth and can prevent further phase-error reduction by simply increasing controller gains. Fig 2 shows a principal control scheme of current high speed pulsers.

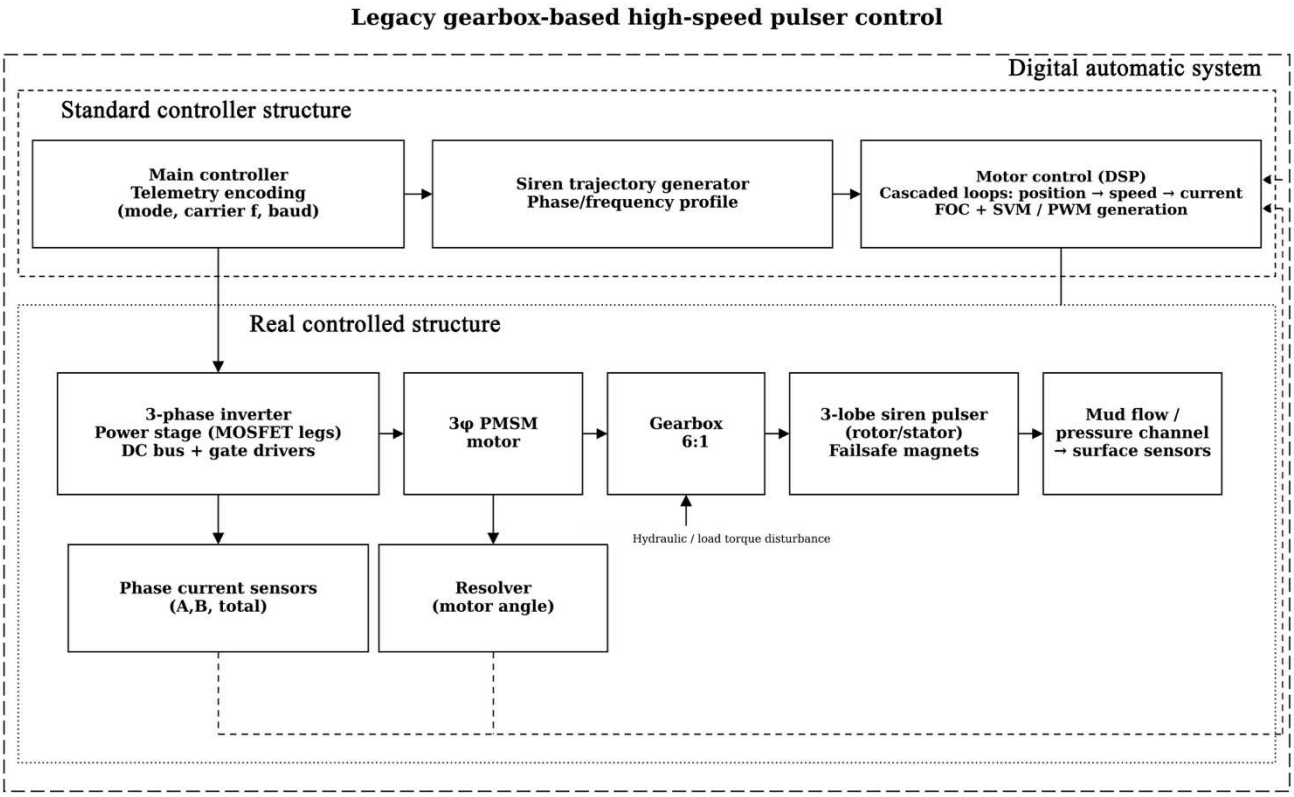


Fig. 2. Block diagram of the legacy gearbox-based control system.

Proposed Solution to Overcome These Limitations

To address the above limitations, we propose a direct-drive siren-type pulser in which the PMSM is coupled directly to the siren rotor and no reduction gearbox is used. Removing the gearbox reduces the number of moving parts and eliminates backlash, while shifting the phase-accuracy challenge to the motor-drive control system. To maintain phase stability under deterministic and rapidly varying load torque, a multiloop covariant vector-control system is developed. The controller combines the baseline cascaded feedback structure with: (i) a virtual-model channel that reduces sensitivity to sensor limitations and (ii) a load-torque invariance block designed using the invariance principle to compensate disturbances caused by the position-dependent hydraulic torque and by the pulser parking

mechanism. The proposed combination of a simplified direct-drive mechanical design and an invariance-based controller enables phase-stable operation for BPSK/QPSK/MSK modulation and supports increased telemetry data rates with reduced manufacturing and maintenance cost.

The objective of this study is to minimize the control error of the electric motor driving a high-speed pulser directly. Since angular error of the motor rotor translates into phase error during signal modulation (e. g., BPSK, QPSK, or MSK), the problem is reduced to implementing highly accurate position-tracking control that minimizes phase mismatch during abrupt phase transitions and under external disturbances. To this end, a multi-loop control architecture [37-42] has been implemented for a permanent-magnet synchronous motor (PMSM) with vector control based on Clarke and Park transformations. This architecture simultaneously utilizes feedback loops for rotor position, angular velocity, and load torque acting on the motor shaft. By explicitly accounting for all three control variables, the system purposefully reduces phase modulation errors, thereby enhancing the fidelity and data rate of the hydraulic telemetry channel.

High-speed siren pulsers are commonly driven by a synchronous motor controlled using a cascaded structure with nested position, speed, and current loops. To achieve phase-stable operation without relying on gearbox stiffness, the baseline structure is extended using a covariant control concept and an invariance block. The resulting multi-loop control architecture is shown in Fig. 3.

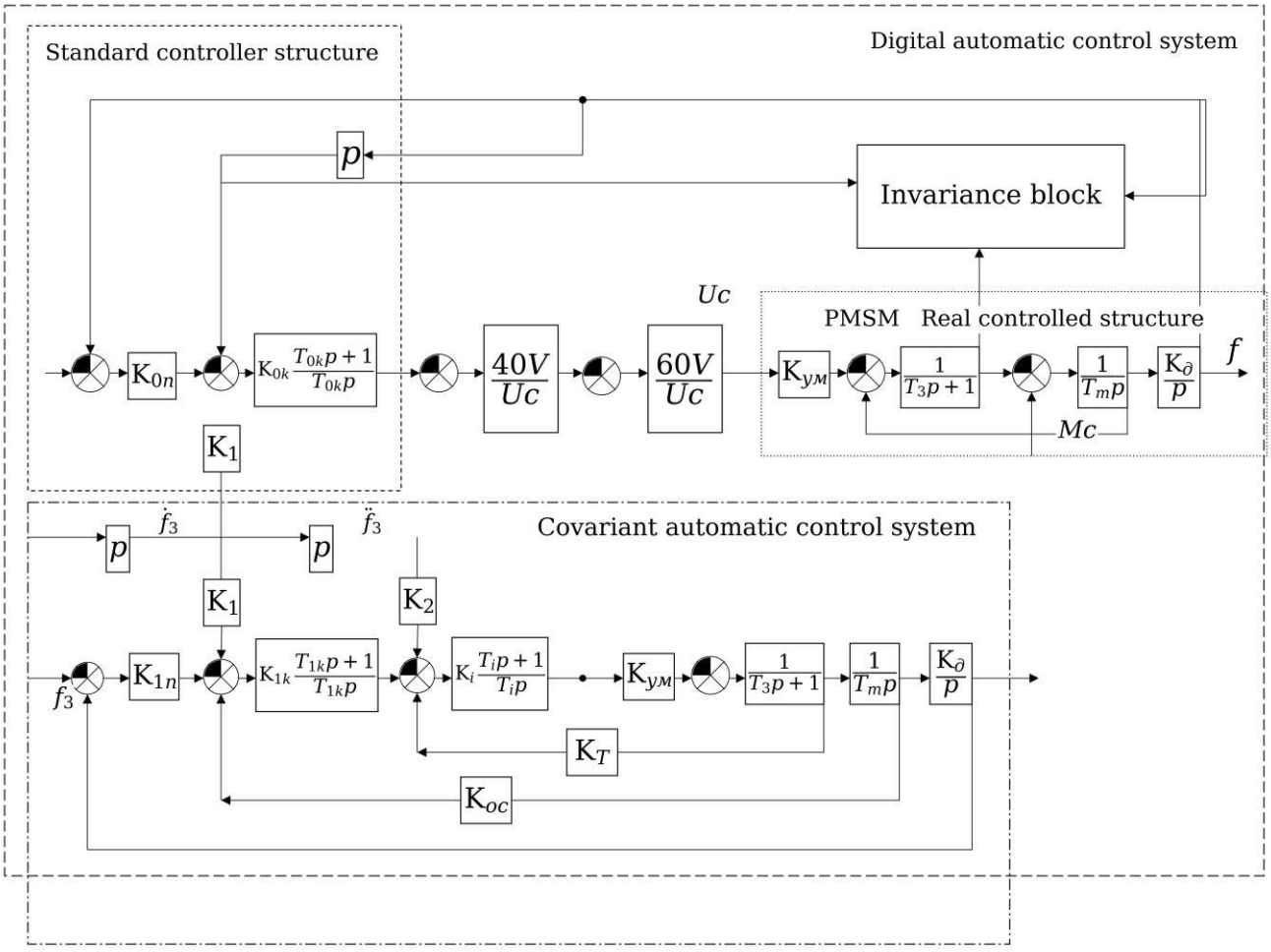


Fig. 3. Block diagram of the proposed multi-loop covariant control system with virtual functionality and load-torque invariance.

Experimental Results and Analysis

Let us now examine the phase modulation control processes within the high-speed pulser control system.

Figure 4 presents the time-domain response of the control system operating with only the "standard regulator structure" block active, while the virtual feedback and load-torque invariance blocks are disabled. The modulation process is shown for the QPSK 20 Hz / 20 baud mode: initially, the rotor accelerates to the speed corresponding to a 20 Hz carrier (54.61333 angle-sensor counts per 2 ms control interval), after which the codes …00, 01, 10, 11… are transmitted sequentially. The vertical axis represents the angle-sensor counts, and the horizontal axis represents the time quanta (2 ms each). In this mode, the maximum control error reaches approximately 80 counts, which is clearly visible from the red curve "angular error."

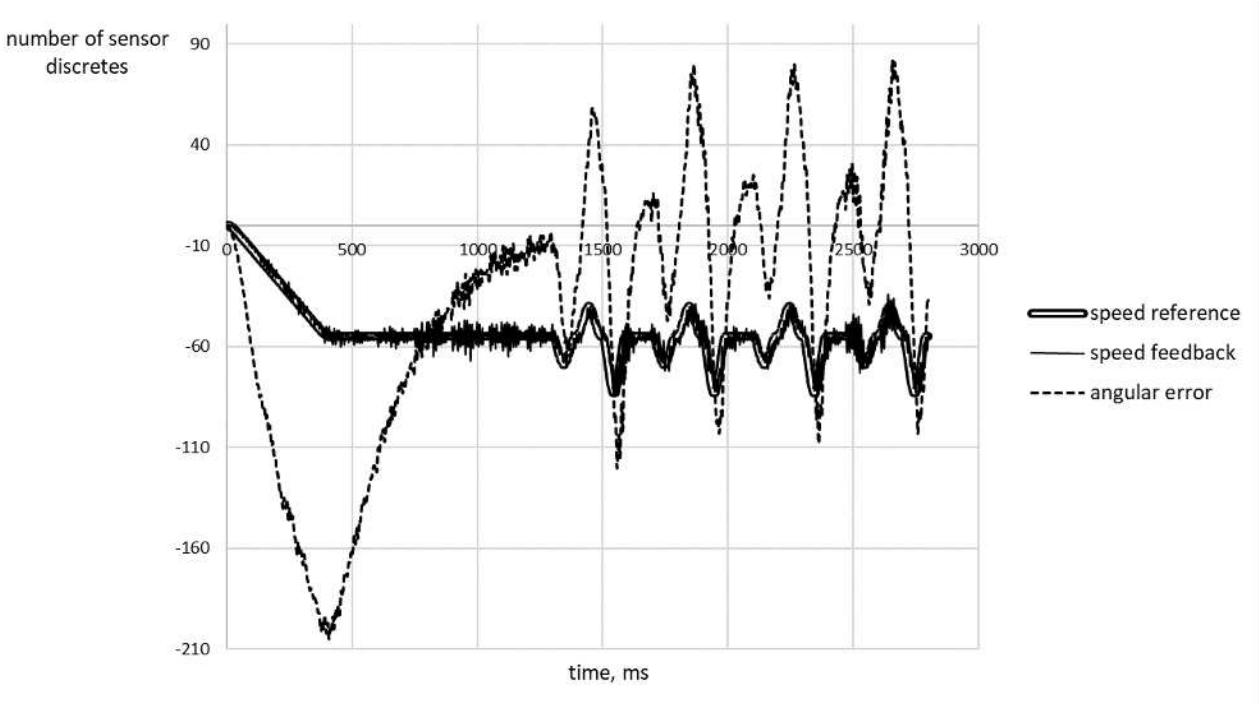


Fig. 4. Time-domain response of the control system enhanced with virtual functionality

In Fig. 4, the speed feedback signal is shown in black. At a control time quantum of 0.002 s, the noise amplitude in this signal is about 5 sensor counts, i.e., approximately 10% of the constant rotational speed (54.61333 sensor counts per control interval of 2 ms). This is close to the limiting compromise in the choice of time quantization and controller gains for the angle and current sensors used in the system.

Attempts to reduce the control error in the system with real feedbacks were unsuccessful. To decrease this error, it is necessary to increase the gain of the speed and position controllers. Without violating system stability, this can only be done by reducing the control time quantum of the controllers. The rotor speed is determined from the increment of the rotor angle over the control time quantum. As the control time quantum is reduced, the accuracy of the speed measurement decreases (the number of quantization levels for the speed amplitude decreases). This, in turn, leads to an increase in the amplitude of pulsations in the control system.

To overcome the limitations imposed by sensor accuracy, a "virtual functionality – covariant-system model" was introduced into the control structure (Fig. 3). The internal model with "ideal" sensors generates a reference control action at the inverter input, while the real system superimposes a corrective component on top of it, taking into account the actual currents, angle, and speed. To formalize the concept of covariant control and to define the conditions under which the steady-state tracking error becomes zero, we consider the analytical representation of the closed-loop regulation error for a system augmented with additional control channels based on the first derivatives of the reference input. This formulation allows explicit derivation of parameter constraints that ensure covariance of the control system.

$$\Delta f(p) = f_z(p)\frac{\sum_{j=1}^{5} p^j(B_j - C_j)}{B_5p^5+B_4p^4+B_3p^3+B_2p^2+B_1p+1}, \qquad (1)$$

where

$$B_5 = \frac{A_4}{K_pK_dK_{oc}^{-1}}, B_4 = \frac{A_3}{K_pK_dK_{oc}^{-1}}, B_3 = \frac{A_2}{K_pK_dK_{oc}^{-1}},$$

$$B_2 = \frac{A_1}{K_p K_d K_{oc}^{-1} + T_k T_i},\ B_1 = \frac{1}{K_p K_d K_{oc}^{-1}} + T_k + T_i,$$

$$A_4 = \frac{T_k \widetilde{T}_i T_m T_e}{K_{oc} K_k K_t^{-1}},\ A_3 = \frac{T_k T_m (\widetilde{T}_i + T_i)}{K_{oc} K_k K_t^{-1}},$$

$$A_2 = T_k \left(\frac{\widetilde{T}_i + T_m}{K_{oc} K_k K_t^{-1}} + T_i \right),\ A_1 = T_k + T_i$$

$$\widetilde{T}_i = \frac{T_i}{K_t K_i K_{um}},$$

$$C_5 = \frac{K_3 T_k T_i}{K_p K_k K_i},\ C_4 = \frac{K_2 T_k T_i}{K_p K_k},\ C_3 = \frac{K_2 T_k}{K_p K_k} + \frac{K_1 T_k T_i}{K_p},$$

$$C_2 = T_k T_i + \frac{K_1 (T_k + T_i)}{K_p},\ C_1 = T_k + T_i + \frac{K_1}{K_p}$$

for the regulation error Δf(p) to be identically zero, the conditions $B_j = C_j$ must be satisfied for j = 1, 2, … , 5. the required parameter settings of the covariant control system that ensure fulfillment of these conditions are determined below. From the condition $B_1 = C_1$, the following equality is obtained

$$\frac{1}{K_p K_d K_{oc}^{-1}} + T_k + T_i = T_k + T_i + \frac{K_1}{K_p}$$

from which the required value of the coefficient K_1 is determined as

$$K_1 = \frac{K_{oc}}{K_d}. \qquad (2)$$

The condition $B_2 = C_2$ is satisfied if the following equality holds:

$$\frac{A_1}{K_p K_d K_{oc}^{-1}} + T_k T_i = T_k T_i + \frac{K_1 (T_k + T_i)}{K_p}$$

Substituting the expression for A_1 into this equality, it can be shown that, if K_1 is equal to the value given by (2), no additional parameter tuning is required to satisfy this condition. The condition $B_3 = C_3$ requires fulfillment of the following identity:

$$\frac{A_2}{K_p K_d K_{oc}^{-1}} = \frac{K_2 T_k}{K_p K_k} + \frac{K_1 T_k T_i}{K_p},$$

From which, after substituting K_1 from (2) and A_2 from (1), the requirement for tuning the parameter K_2 follows as:

$$K_2 = \frac{\widetilde{T}_i + T_m}{K_d K_t^{-1}}. \qquad (3)$$

To satisfy the condition $B_4 = C_4$, the following equality must hold:

$$\frac{A_3}{K_p K_d K_{oc}^{-1}} = \frac{K_2 T_k T_i}{K_p K_k},$$

From which, after substituting K_2 from (3) and A_3, it follows that:

$$T_m (\widetilde{T}_i + T_i) = T_i (\widetilde{T}_i + T_m).$$

This equality is satisfied when the following parameter setting is applied:

$$T_i = T_m. \qquad (4)$$

The condition $B_5 = C_5$, which has the form:

$$\frac{A_4}{K_p K_d K_{oc}^{-1}} = \frac{K_3 T_k T_i}{K_p K_k K_i},$$

defines the tuning of parameter K_3 as:

$$K_3 = \frac{T_m T_e}{K_{um} K_d}. \qquad (5)$$

It should be noted that the parameter settings defined by equations (2)–(5) ensure zero regulation error only under the assumption that all additional control channels associated with the derivatives of the reference signal operate within admissible limits. In practical implementations, the magnitude of derivative-based signals must remain bounded to guarantee stable and physically realizable operation of the control system. Figure 4 shows the time-domain waveforms of the formation of the reference inputs f_3, $\dot{f}_3$, $\ddot{f}_3$, $\dddot{f}_3$.

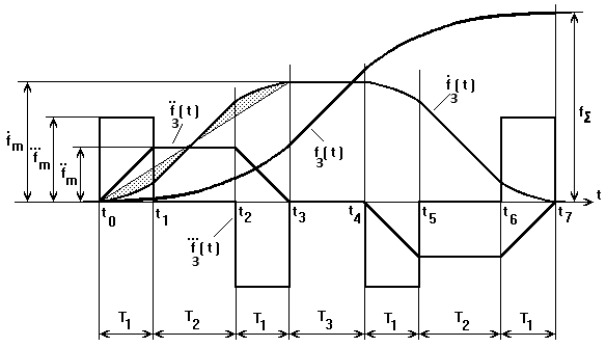


Fig. 5. Time-domain waveforms of the reference signal during a modulation phase step.

In practice, full covariance (zero regulation error) cannot be achieved due to the following factors: amplitude and time quantization inherent to the digital control system; parameter variations of the converter–motor power stage, which limit the accuracy of conditions (2)–(3); uncontrolled disturbance inputs (load torque); nonlinear behavior of system elements, including the power converter and input signal formers.

The internal model with “ideal” sensors generates a reference control input to the inverter, whereas the real system adds a corrective component that accounts for the

measured currents, rotor angle, and speed. Under the same QPSK 20 Hz / 20 baud operating conditions, the error is reduced by almost a factor of three — from ~80 to ~30 counts. This result demonstrates that combining the reference (model-based) control action with the corrective (measurement-based) contribution makes it possible to effectively "bypass" position-sensor quantization in terms of control error. In this configuration, the pulser successfully passed test-bench and field trials under downhole drilling conditions.

The next step addresses a real operational factor—the parking mechanism, which uses permanent magnets to generate an alternating (sign-changing) load torque on the motor shaft. In the previous time-domain plots (Figs. 2), this parking mechanism was inactive. However, when engaged, the parking torque periodically decelerates or accelerates the rotor depending on its angular position, introducing a significant periodic disturbance.

As a result, the regulation error increases substantially. In Figs. 4, the time-domain waveforms of the transient processes in the modulator with the parking mechanism are shown, where only two subsystems — those with real and virtual feedback — are operating (see Fig. 3). At a modulation frequency of 20 Hz, the use of the parking mechanism results in control errors of approximately 100–125 counts. At a modulation frequency of 1 Hz, the error becomes excessive, reaching approximately 300–325 counts (Fig. 6). These results clearly demonstrate that even a highly accurate reference model alone is insufficient to maintain precise phase control in the presence of systematic, position-dependent load torque disturbances.

To eliminate the impact of this disturbance, a load-torque invariance block was introduced (Fig. 3). The key feature of this approach lies in the fact that the disturbing torque is not random but deterministically dependent on the rotor angle. During steady-state rotation, a calibration procedure is performed to map the relationship "rotor angle → required compensating current." This results in a lookup table containing 4096 pre-recorded current values, corresponding to the full resolution of the position sensor. During operation, the current rotor angle determines the index in this lookup table. Taking into account the current rotational speed and the necessary phase lead, the index is shifted forward in time to anticipate the upcoming disturbance. The selected compensating current value is then scaled by a gain factor and added to the main control signal as a feedforward (anticipatory) compensation term. Essentially, this implements a feedforward channel that proactively counteracts the known, angle-dependent disturbance, thereby significantly reducing the burden on the feedback loops. The effectiveness of the invariance block is clearly demonstrated in Fig. 7. In all cases, the red curve (angular error) is substantially reduced compared to the scenarios without invariance (Fig. 6), while the blue current curves maintain similar amplitudes. This observation is significant because, without the invariance block, the system must compensate for the disturbance reactively, using currents of comparable magnitude but only *after* the error has already accumulated. In contrast, the feedforward compensation preemptively neutralizes the disturbance, minimizing phase error before it occurs.

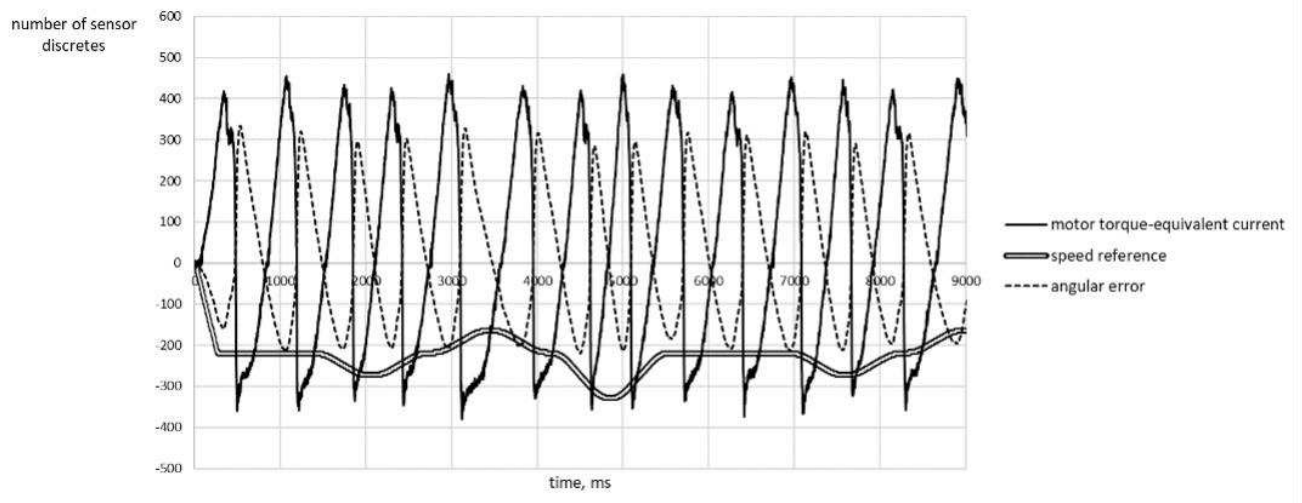


Fig. 6. Time-domain response of the system with the parking mechanism engaged at a carrier frequency of 1 Hz (red – angular error; blue – motor torque-equivalent current; black – speed reference).

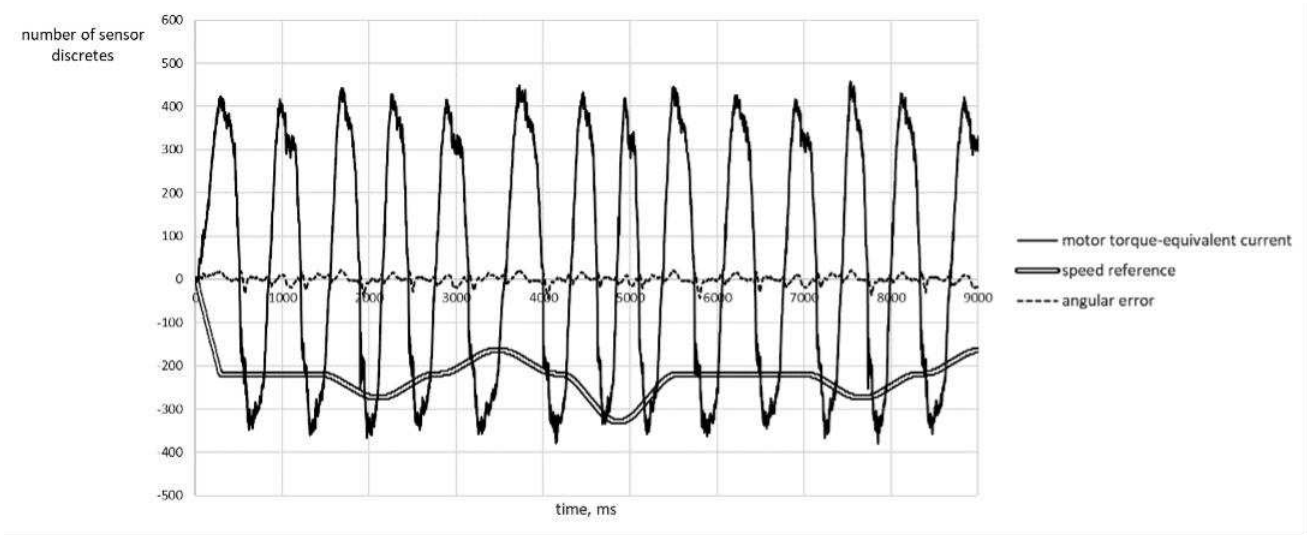


Fig. 7. Time-domain response of the system with the parking mechanism engaged at a carrier frequency of 1 Hz (red – angular error; blue – motor torque-equivalent current; black – speed reference). The "standard regulator structure," "virtual system," and "invariance" blocks are all active.

Measurement error analysis

To interpret the experimental tracking-error traces, the measured regulation error is compared with the finite resolution of the digital feedback signals used in the control loops. In the present drive, rotor angle, phase current, and speed are represented in discrete counts; therefore their quantization sets a lower bound for the achievable error. For an ideal mid-tread quantizer, the quantization error εq can be modeled as a random variable uniformly distributed on the interval [−0.5, +0.5] LSB. In this case, the equivalent standard deviation is σq = 1/√12 ≈ 0.289 LSB, and the corresponding 3σ interval is 3σq ≈ 0.866 LSB.

(i) Rotor angle. The position sensor resolution is 4096 counts per revolution (1 count = 360/4096 = 0.0879°). Thus, the quantization bound is ±0.5 count (±0.044°), whereas the equivalent 3σ level is 0.866 count (0.076°).

(ii) Phase current. Based on the drive calibration, 1240 ADC counts correspond to 20 A full scale (1 LSB = 20/1240 = 0.0161 A). The quantization bound is therefore ±0.0081 A, and the equivalent 3σ level is ≈0.0140 A.

(iii) Speed. The speed feedback is obtained by finite-difference differentiation of the quantized rotor angle over the control time quantum Ts = 2 ms. One LSB of speed therefore corresponds to nLSB = (60/(4096·Ts)) = (500·60)/4096 = 7.324 rpm, and the equivalent 3σ level is 6.34 rpm. The ≈5-count jitter observed in the speed trace (Fig. 4) should not be interpreted as the intrinsic sensor error, because it also includes the effects of numerical differentiation, drive dynamics, and disturbance torque.

The regulation error in Figs. 6–7 is expressed in the same encoder counts; conversion to degrees uses θ[deg] = count·360/4096. Because the error is strongly affected by deterministic phase steps and periodic load torque, its distribution is generally non-Gaussian. Therefore, in addition to min/max and RMS values, an empirical 99.73% coverage interval is reported (analogous to a ±3σ interval for a Gaussian process). Without invariance compensation (Fig. 6), the error ranges from −222 to +340 counts, with a peak of 340 counts (29.9°) and RMS = 168.1 counts (14.8°). The empirical 99.73% interval is [−220, +334.85] counts (−19.34° to +29.43°). With invariance compensation enabled (Fig. 7), the error is reduced to −44 to +22 counts, with a peak of 44 counts (3.87°) and RMS = 9.73 counts (0.855°). The empirical 99.73% interval becomes [−41, +21] counts (−3.60° to +1.85°).

In both cases, the observed regulation error exceeds the angle-sensor quantization bound (±0.5 count) by nearly two orders of magnitude. Hence, the contribution of position quantization to the displayed error traces is negligible, and it does not affect the comparative conclusion regarding the benefit of invariance-based disturbance compensation.

Reliability and limitations

Over time, the high-coercivity magnets used in the motor and parking mechanism lose part of their remanent magnetic flux density (demagnetize). The modulator control system therefore includes an automatic update mode for the "angle → compensating current" lookup table. Periodic execution of this procedure during pulsator

maintenance allows the negative impact of magnet aging to be partially compensated for a certain period. From a practical standpoint, the proposed control architecture—a multi-loop covariant control architecture enhanced with virtual functionality and load-torque invariance—delivers the required phase stability for high-density modulation schemes (BPSK/QPSK/MSK) in mud-pulse telemetry applications. Laboratory and field tests have demonstrated a physical data transmission rate exceeding 6 bits/sec. When combined with advanced data compression algorithms, the system achieves an effective throughput of over 50 bits/sec. This performance level is sufficient to support real-time operation of triple-combo logging-while-drilling (LWD) tool strings and enables expansion of the real-time geophysical measurement suite during drilling operations.

The pulser is currently undergoing field testing to accumulate statistically significant data for estimating mean time between failure (MTBF) and maintenance cost in accordance with industry standards. Estimated MTBF is >10 000 circulation hours, which is higher more than 20% of the most reliable legacy pulsers. A key advantage of the proposed design, relative to existing high-speed pulsers, is its lightweight mechanical architecture employing a direct-drive configuration. The manufacturing and maintenance cost of the new pulser is 15–20% lower than that of current high-speed pulsers, primarily due to the elimination of the gearbox.

Integration into Existing MWD Systems

The proposed high-speed pulser is designed to be compatible with the architecture of current MWD systems in which the pulser acts as the primary downhole actuator for the telemetry channel. Integration into an existing toolstring typically requires coordination at three levels: mechanical/hydraulic interfaces, downhole electronics and firmware, and the surface decoding chain.

Economic impact

In recent years, global drilling activity has remained substantial. According to Rystad Energy, around 70,000 new oil and gas wells were drilled globally in 2023 at a total cost of about $325 billion, and roughly 2 million wells have been completed worldwide since 2000 [43]. This level of activity creates a large and recurring demand for reliable MWD/LWD and telemetry equipment, and even incremental improvements in downhole telemetry availability and maintenance cost can translate into significant aggregate savings across the industry.

From a cost and operational perspective, the direct-drive concept targets both tool economics and drilling efficiency. Eliminating the reduction gearbox simplifies the mechanical design and reduces the number of moving parts. In our development program, this simplification reduced manufacturing and maintenance cost by approximately 15–20% compared with gearbox-based designs, while also reducing sensitivity to wear-related phase drift. A conservative estimate assumes a unit manufacturing cost of approximately USD 80,000 per high-speed pulser. For a worldwide installed base of roughly 60,000 telemetry tools, direct replacement of existing pulsers would therefore represent a one-time manufacturing cost reduction on the order of USD 720 million. In addition, assuming an annual spare parts and maintenance cost of approximately 15% of the pulser value, the transition would yield a further recurring saving of about USD 108 million per year. Beyond direct manufacturing and maintenance economics, improved operational reliability, higher telemetry quality, and reduced non-productive time (NPT) constitute a critical financial driver for oil and gas operators and should be considered as an additional, potentially dominant component of the overall economic impact.

References

[1] Zhdaneev, O. V. Technological and institutional priorities of the oil and gas complex of the Russian Federation in the term of the world energy transition / O. V. Zhdaneev, K. N. Frolov // International Journal of Hydrogen Energy. – 2024. – Vol. 58. – P. 1418-1428. – DOI 10.1016/j.ijhydene.2024.01.285. – EDN PLLMKU.

[2] U.S. Energy Information Administration (EIA). Monthly Energy Review. 2025.

[3] Su F., Guo S., Zhang J. Mud pulse telemetry: current achievements and challenges. Applied Sciences. 2024.

Zhang H., Zhao Y., Guo F., Bao Y. Study on open-hole extended-reach limit in horizontal drilling. Energy Science & Engineering. 2024. DOI: 10.1002/ese3.1703

[4] Zhang J., Fan Z. Key technologies for increasing production based on best practices of major shale oil and gas basins. Energy Geoscience. 2025. DOI: 10.1016/j.engeos.2025.100414

[5] Ghosh D. A review of basic well log interpretation techniques in highly deviated wells. Journal of Petroleum Exploration and Production Technology. 2022. DOI: 10.1007/s13202-021-01437-2
[6] Gravley W. Review of Downhole Measurement-While-Drilling Systems. Journal of Petroleum Technology. 1983. DOI: 10.2118/10036-PA
[7] Cai Z., Zhou B., Fu Z., Zhang S. Research on the development trends of measurement while drilling (MWD) technology. Petroleum Science. 2025. DOI: 10.1016/j.petsci.2025.12.013
[8] Bittar M., Plumb C., Santos E., Li L. A new azimuthal deep-reading resistivity tool for geosteering and advanced formation evaluation. SPE Annual Technical Conference and Exhibition. 2007.
[9] Zhdaneev O.V., Zaytsev A.V., Prodan T.T. Possibilities for creating Russian high-tech bottomhole assembly // Journal of Mining Institute. – 2021. – Vol. 252. – P. 872-884. – DOI: 10.31897/PMI.2021.6.9
[10] Zhdaneev O.V., Frolov K.N. Drilling technology priorities in Russia // Neftyanoe Khozyaystvo - Oil Industry. 2020. – P. 42-48. – DOI: 10.24887/0028-2448-2020-5-42-48
[11] Zhdaneev O.V., Zaitsev A.V., Lobankov V.M. Metrological support of equipment for geophysical research // Journal of Mining Institute. 2020. Vol. 246. p. 667-677. DOI: 10.31897/PMI.2020.6.9
[12] Li C., Xu Z. A review of communication technologies in mud pulse telemetry systems. Electronics. 2023. DOI: 10.3390/electronics12183930
[13] Halldorson J. A., Potter R., Killalea R., Rieck G. Wired drill-pipe telemetry for high-data-rate MWD applications: field results. SPE Annual Technical Conference and Exhibition. 1993. DOI: 10.2118/24971-MS
[14] Cooper P., Santos L. S. B. New mud-pulse telemetry system delivers improved drilling dynamics and formation evaluation data. SPE Russian Petroleum Technology Conference. 2015.
[15] Su Y., Sheng L., Li L., Bian H., Shi R., Chin W. High-data-rate measurement-while-drilling system for very deep wells. AADE National Technical Conference and Exhibition. 2011.
[16] Caruso D., Candler S., Brunton A., Leger P. High data rate mud pulse telemetry and turbine alternator for deepwater operations. Offshore Technology Conference. 2012.
[17] Yan Z., Guo P., Wang X., Wu G. Design of a rotary valve orifice for a continuous wave mud pulse generator and analysis of the signal characteristics. Precision Engineering. 2015. DOI: 10.1016/j.precisioneng.2015.03.005
[18] Shao J., Wang L., Zhang S., Liu M. Differential signal extraction algorithm for continuous wave mud pulse telemetry. Journal of Petroleum Science and Engineering. 2017. DOI: 10.1016/j.petrol.2016.09.047
[19] Tu B., Li D., Lin E. H., Ji M. Research on mud pulse signal data processing in MWD. EURASIP Journal on Advances in Signal Processing. 2012. DOI: 10.1186/1687-6180-2012-182
[20] Wu A., Zhang M., Mwachaka S., Fu Q. Continuous phase-frequency keying modulation and adaptive coherent detection method for mud pulse telemetry systems. Digital Signal Processing. 2021. DOI: 10.1016/j.dsp.2021.103162
[21] Zhang J., Chen L., Yu S., Xia H., Yan G. Noise cancellation method for mud pulse telemetry based on discrete Fourier transform. Journal of Marine Science and Engineering. 2025. DOI: 10.3390/jmse13010075
[22] Han H., Cao X., Zhang Q. Transient flow analysis in natural gas pipelines for high-rate mud pulse telemetry in rotary steerable system. Journal of Natural Gas Science and Engineering. 2024. DOI: 10.1016/j.jngse.2023.108274
[23] Derendyaev A. A., Fatyanov A. V. High-speed downhole telemetry system for monitoring drilling equipment parameters and real-time drilling process control. Geomodel 2023. 2023.
[24] Bamisebi A. A., Deng Y., Li M., Yao M., Guo Y. Advancements in mud pulse telemetry: a review of data acquisition and transmission techniques in drilling operations. Discover Applied Sciences. 2025.
[25] Bamisebi A. A., Deng Y., Guo Y., Li M. Improving mud pulse telemetry communication speeds through compressed sensing. International Conference on Data Analytics for Business and Industry. 2022.
[26] Su J., Li D., Shao J. Mud pulse telemetry based on combined coding and the high-speed drive technology of mud pulser. Journal of Signals and Systems Engineering. 2014.
[27] Lerner D., Masak P. Integrated modulator and turbine-generator for a measurement while drilling tool. U.S. Patent US5517464A. 1996.

[28] Montaron B. Methods and devices for real-time formation imaging through measurement while drilling telemetry. U.S. Patent US5519668A. 1996.
[29] Malone D., Johnson M. Logging while drilling tools, systems, and methods capable of transmitting data at a plurality of different frequencies. U.S. Patent US5375098A. 1994.
[30] Hahn D., Peters V., Rouatbi C., Eggers H. Oscillating shear valve for mud pulse telemetry. U.S. Patent US7280432B2. 2007.
[31] Seyler T., Wisler M. Adjustable shear valve mud pulser and controls therefor. U.S. Patent USRE40944E1. 2009.
[32] McDonald C. R., Stewart J., Chadwick R. Measurement-while-drilling system and method. U.S. Patent US5583827A. 1996.
[33] Fails G. A. Mud-operated pulser. U.S. Patent US5586084A. 1996.
[34] Padman R., Wang M. Pulser. U.S. Patent US6237793B1. 1999.
[35] Pittman M. Rotary acting shear valve for drilling fluid telemetry systems. U.S. Patent US4565132A. 1986.
[36] Walsh B., Stroud J. Rotary pulser for transmitting information to the surface from a drill string down hole in a well. U.S. Patent US7350542B2. 2008.
[37] Quang N. D., van Gerven B., Weber J., Gervasoni J., Girotti G., Quoilin S. A review on position control of permanent magnet synchronous motor: from classic PID to industry-standard field-oriented control. Journal of Electrical Systems. 2023.
[38] Apte R., Bhangale P. G., Chaudhari M. Implementation of digital signal controller based PMSM drive for speed control for water pump application. IEEE International Conference on Automation, Control and Applications. 2015.
[39] LaSalle J. P. Some extensions of Lyapunov's second method. IRE Transactions on Circuit Theory. 1960. DOI: 10.1109/TCT.1960.1086720
[40] Gray R. M., Neuhoff D. L. Quantization. IEEE Transactions on Information Theory. 1998. DOI: 10.1109/18.720541
[41] Peng L., Prodic A., Alarcon E., Maksimovic D. Modelling of quantization effects in digitally controlled PWM converters. IEEE Power Electronics Specialists Conference (PESC). 2004.
[42] Takahashi I., Noguchi T. A new quick-response and high-efficiency control strategy of an induction motor. IEEE Transactions on Industry Applications. 1986. DOI: 10.1109/TIA.1986.4504799
[43] Rystad Energy. Wells in focus: Overview of global well activity. 2024.